Tyr is Responsible for the *Cctq1a* QTL and Links Developmental Environment to Central Corneal Thickness Determination

Kacie J. Meyer[1§], Demelza R. Larson[1§], S. Scott Whitmore[2], Carly J. van der Heide[1,2], Adam Hedberg-Buenz[1,3], Laura M. Dutca[3], Swanand Koli[4], Nicholas Pomernackas[1], Hannah E. Mercer[1], Maurisa N. Mansaray[1], William J. Paradee[5], Kai Wang[6], K. Saidas Nair[4,7], Todd E. Scheetz[2], and Michael G. Anderson[1,2,3]*

[1]Department of Molecular Physiology and Biophysics, University of Iowa, Iowa City, Iowa; [2]Department of Ophthalmology and Visual Sciences, University of Iowa, Iowa City, Iowa; [3]Center for the Prevention and Treatment of Visual Loss, Iowa City VA Health Care System, Iowa City, Iowa; [4]Department of Ophthalmology, University of California, San Francisco, California; [5]Genome Editing Core Facility, University of Iowa, Iowa City, Iowa; [6]Department of Biostatistics, University of Iowa, Iowa City, Iowa; [7]Department of Anatomy, University of California, San Francisco, California

[§]Equal contribution

*Corresponding author: Dr. Michael G. Anderson, Department of Molecular Physiology and Biophysics, 3123 Medical Education and Research Facility, 375 Newton Road, Iowa City, IA 52242, (319) 355-7839 (telephone), (319) 335-7330 (FAX), michael-g-anderson@uiowa.edu

Abstract

Central corneal thickness is a quantitative trait with important associations to human health. In a phenotype-driven approach studying corneal thickness of congenic derivatives of C57BLKS/J and SJL/J mice, the critical region for a quantitative trait locus influencing corneal thickness, *Cctq1a*, was delimited to a 10-gene interval. Exome sequencing, RNAseq, and studying independent mutations eliminated multiple candidate genes and confirmed one. Though the causative gene, *Tyr*, has no obvious direct function in the transparent cornea, studies with multiple alleles on matched genetic backgrounds, both in isolation and genetic complementation crosses, confirmed allelism of *Tyr*-*Cctq1a*; albino mice lacking *Tyr* function had thin corneas. Albino mice also had increased axial length. Because albinism exposes eyes to increased light, the effect of dark-rearing was tested and found to rescue central corneal thickness. In sum, the results point to an epiphenomenon; developmental light exposure interacts with genotype as an important determinate of adult corneal thickness.

Introduction

Central corneal thickness has important associations with ocular disease, but its natural determining factors remain predominately elusive. The cornea consists of three cellular layers (an outermost epithelium, middle stroma, and innermost endothelium) separated by two thinner basement membranes. The combined central thickness of these layers (central corneal thickness, CCT) increases rapidly through infancy and early childhood, reaches adult values in pre-teen ages, and remains relatively stable thereafter, with eventual modest age-related thinning[1, 2, 3, 4]. For largely unknown reasons, average CCT can vary by dozens of microns between ethnicities[4, 5]. Thin CCT is associated with several corneal diseases, such as corneal dystrophy, brittle cornea syndrome, keratoconus, and cornea plana; diseases of connective tissue, such as Marfan syndrome, Ehlers-Danlos syndrome, Loeys-Dietz syndrome, and osteogenesis imperfecta; and at least two diseases in which the nature of, and/or reason for, the association is unclear, including myopia and primary open angle glaucoma[6].

CCT is a highly heritable trait[7, 8], leading to many genetic studies. Variants influencing CCT have been identified from familial studies of Mendelian syndromes and GWAS of various large populations[9, 10, 11, 12]. From these studies, some themes have begun to emerge. For example, some of the same CCT loci are identified in both multigenic and Mendelian disease studies[10, 13, 14]. It has also been common to identify variants related to collagen matrix integrity[10, 12, 14, 15]. However, it is also clear that much remains unknown. Among the known associations, most known SNPs occur in non-coding regions, and the nearest genes typically have no obvious link to known structural components of the cornea[15]. It is also clear that many important genes remain to be discovered. Known SNPs give rise to a SNP-based heritability estimate of 42.5% and account for only 14.2% of the CCT variance[9].

Here, an unique approach complementary to others is undertaken using inbred mouse strains to identify quantitative trait loci (QTL) that influence CCT[16]. Similar to humans, there is natural variation of CCT among inbred mouse strains[17]. Previous work using a quantitative approach with intercrosses between two such strains (C57BLKS/J [KS] mice with thin corneas and SJL/J [SJL] mice with thick corneas) identified the first CCT QTL, *Central corneal thickness QTL 1* (*Cctq1*) on mouse chromosome 7[16]. Here, *Cctq1* was resolved into two closely linked regions, *Cctq1a* and *Cctq1b*, which each influence CCT. Through multiple genetic approaches, a mutation in the tyrosinase gene (*Tyr*) is identified as causative of the *Cctq1a* phenotype, which appears to influence CCT via an epiphenomenon dependent on developmental light exposure.

Results

Cctq1 contains two adjacent interacting QTL

The original 95% Bayesian credible interval of *Cctq1* spanned a 38.3 cM region on chromosome 7 (34.1 cM – 72.4 cM)[16]. To reduce this interval, recombination mapping was used with 92 recombinant N4 intercross mice. However, the interval was originally recalcitrant to division—more than one interval conferred the increased CCT phenotype. This suggested that there was too much genetic heterogeneity for this trait at the N4 generation, potentially including the presence of more than one CCT-regulating gene within or near *Cctq1*. To address these possibilities, the original F2 dataset was subjected to additional evaluations while backcrossing of the congenic mice to the N10 generation was continued.

The original analysis of (KS X SJL) F2 mice was based upon a significance threshold determined empirically by stratified permutation testing with 1000 permutations[16, 18], and did not identify any loci that significantly interacted with *Cctq1*. Prompted by the recombination

mapping, the dataset was re-examined by performing a pairwise scan of the markers on chromosome 7 using scantwo analysis with R/qtl[18, 19]. Of the possible interactions, the markers that produced the highest LOD scores were *D7Mit31* and *rs13479535* (Figure 1A; full LOD score = 10.33, interactive LOD score = 5.05). *D7Mit31* lies within the 95% Bayes credible interval of *Cctq1*; *rs13479535* is 2 cM distal to the end of the interval at 74.3 cM. The putative linked loci were subsequently subjected to multiple regression analysis in which each locus and the interaction component were sequentially dropped from the 2-QTL model. This analysis indicated that both loci and their interaction had significant contributions to the model (Supplementary Data 1). The QTL at *D7Mit31* was responsible for 31% of the phenotypic variability while the QTL at *rs13479535* accounted for another 24% of the variability. These data indicate that both loci are true QTL. *Cctq1* was thus resolved into two QTL, *Cctq1a* (95% Bayes credible interval: *D7Mit318–D7Mit220*, spanning 49.0 cM, peak at *D7Mit31*), and *Cctq1b* (95% Bayes credible interval: *D7Mit105–rs13479545*, spanning 74.3 cM, peak at *rs13479535*; Figure 1B).

To reduce genetic heterogeneity, N4 mice were further backcrossed onto the KS background to the N10 generation. Because the congenic interval was relatively large, a panel of six markers was used at each generation of backcrossing to keep the interval intact. At generation N10, congenic mice were intercrossed, recombination within the interval was allowed, and mice with all nine genetic combinations of *Cctq1a* and *Cctq1b* were phenotyped for CCT (Table 1). Congenic control mice (KS.SJL-$Cctq1a^{KS}$,$Cctq1b^{KS}$) had a CCT indistinguishable from inbred KS mice (94.8± 2.4 µm vs. 94.5 ± 3.2 µm, respectively; one-way ANOVA with Tukey post-test; Table 1). Congenic mice with SJL genotypes at *Cctq1a* (*i.e.*, KS.SJL-$Cctq1a^{SJL}$) had significantly thinner corneas than inbred KS mice (87.9 ± 3.8 µm; $n = 39$; $p < 0.001$; Student's two-tailed *t*-test) independent of the genotype at *Cctq1b* ($n = 13$ and $p < 0.05$ for each of three genotypes at *Cctq1b*; one-way ANOVA with Tukey post-test; Table 1; Supplementary Data 2). The difference

in thickness mediated by *Cctq1a* is predominantly due to the thickness of the stroma (Δ 9.6 µm, $p < 0.001$; Student's two-tailed *t*-test), though there is a small (Δ 1.2 µm) and marginally significant ($p = 0.022$ Student's two-tailed *t*-test) decrease in thickness of the epithelium as well. Congenic mice with KS genotypes at *Cctq1a* and SJL genotypes at *Cctq1b* (i.e., KS.SJL-$Cctq1a^{KS}$,$Cctq1b^{SJL}$) also had significantly thinner corneas (90.8 ± 2.6 µm; $n = 13$ mice; $p < 0.05$; one way ANOVA with Tukey post-test) than inbred KS mice (Table 1, Supplementary Data 2). No other genetic combinations caused significant changes in CCT compared to inbred KS controls. As predicted from the analysis of the original F2 Dataset with R/qtl, these data with congenic mice independently support that both *Cctq1a* and *Cctq1b* are true QTL capable of altering the phenotypic variability of CCT on a uniform genetic background.

Mapping of *Cctq1a* using recombination mapping and sub-congenics

Because of its larger effect, initial efforts were focused on fine-scale mapping for *Cctq1a*. To identify the gene underlying *Cctq1a*, *Cctq1a*-recombinant N10F2 mice, with KS genotypes at *Cctq1b*, were used to narrow the critical region. From this recombination analysis, the gene underlying *Cctq1a* was deduced to be between SNP markers *rs108403472* at 48.51 cM and *rs6247100* at 50.26 cM. Simultaneously, sub-congenic mice were created by continued backcrossing of the KS.SJL-$Cctq1a^{HET}$;$Cctq1b^{KS}$ N10 mice. Eyes of N10 congenic mice were overtly healthy, differing only in pigmentation between genotypes (Supplementary Data 2). At N12, *Cctq1a* was physically reduced to a 15.9 cM region (KS.SJL-*Cctq1a(15.9cM)*) flanked by *D7mit347* and *D7mit321* and characterized by an association of SJL homozygosity with decreased CCT (87.6 ± 2.3 µm vs. 76.8 ± 2.4 µm, $n = 15$ mice per genotype, $p < 0.001$, Student's two-tailed *t*-test). At N15, *Cctq1a* was physically reduced to a 9.9 cM region (KS.SJL-*Cctq1a(9.9cM)*) flanked by *rs3672782* and *D7mit321*; again characterized by an association of SJL homozygosity with decreased CCT (91.6 ± 2.2 µm vs. 80.7 ± 2.9 µm, $n = 7$ mice per genotype, $p < 0.001$, Student's two-tailed *t*-test). One N15F2 mouse harbored a recombination

event within the minimal sub-congenic interval. The phenotype of this mouse indicated the gene underlying *Cctq1a* lies proximal to marker *rs13479393* (Figure 2). Using this recombinant mouse in a progeny test, additional intercrossing to generation N15F7 confirmed the distal breakpoint proximal to marker *rs13479393* at 49.65 cM, again characterized by an association of SJL homozygosity with decreased CCT (85.7 ± 1.6 μm vs. 94.4 ± 3.3 μm, n = 8–10 mice per genotype; $p < 0.001$, Student's two-tailed t-test; Figure 3A; Supplementary Data 3–5).

In sum, physical recombination mapping utilizing multiple generations of congenic and sub-congenic mice conclusively indicated that the gene underlying *Cctq1a* lies on chromosome 7 between markers *rs108403472* at 48.51 cM and *rs13479393* at 49.32 cM, a 0.81 cM region containing the entirety of eight RefSeq genes (*Vmn2r78*, *Vmn2r79*, *Nox4*, *Tyr*, *Grm5*, *Ctsc*, *Rab38*, and *Tmem135*), the 3' portion of one gene (*Vmn2r77*), and the 5' portion of one gene (*Fzd4*) (Figure 2).

Candidate identification and prioritization

To identify all the possible exonic variants within the *Cctq1a* critical region, whole exome sequencing was conducted on KS and SJL inbred mice. In the entire exome, 15,261 missense, frameshift, and splice-site mutations were found between KS and SJL (Supplementary Data 6). There were six amino acid altering variants within the *Cctq1a* critical region, located within *Vmn2r79* (A223T, L243M, T257I, I265V), *Tyr* (C103S), and *Fzd4* (F27L). Vomeronasal receptor genes, such as *Vmn2r79*, have an increased rate of coding sequence variants [20] and the four altered residues between KS and SJL in *Vmn2r79* are poorly conserved. The amino acid change in *Tyr* from cysteine to serine is the albinism-causing Tyr^{c} allele conferred by the albino SJL strain. The *Fzd4* amino acid variant is within the signal sequence of the protein; KS mice conferred the phenylalanine amino acid residue (the same residue as C57BL/6J mice) while SJL mice conferred the mammalian-conserved leucine residue.

Transcriptional profiling was additionally used to prioritize candidates. Using previously published microarray data comparing adult corneal RNA expression profiles in KS and SJL mice[17], *Nox4*, *Ctsc*, *Rab38*, *Tmem135*, and *Fzd4* were all present in the adult cornea; there was no evidence for adult corneal expression of *Vmn2r77*, *Vmn2r78*, *Vmn2r79*, *Tyr*, or *Grm5*. Of those expressed, *Nox4, Ctsc, and Fzd4* showed differential expression between the two strains. *Nox4* and *Ctsc* were both down-regulated 2.5-fold in SJL, while *Fzd4* was up-regulated 1.6-fold in SJL.

Additionally, RNAseq was performed on corneas of 3-week-old KS.SJL-*Cctq1a(15.9cM)*^{SJL} N12F3 mice. Analysis was focused on three comparisons: 1) KS.SJL-*Cctq1a(15.9cM)*^{SJL} vs. KS (experimental, identifying genes with altered corneal expression in the congenic interval), 2) KS.SJL-*Cctq1a(15.9cM)*^{SJL} vs. KS.SJL-*Cctq1a(15.9cM)*^{KS} (experimental, also identifying genes with altered corneal expression in the congenic interval), and 3) KS.SJL-*Cctq1a(15.9cM)*^{KS} vs. KS (control, identifying genes in the background of the congenic strain with altered corneal expression not associated with the congenic interval) (Supplementary Data 7). In each comparison, genes were first filtered for those with a Q-value ≤ 0.001 and a FPKM ≥ 1 in at least one of the strains. Gene lists were subsequently compared to one another, identifying 87 genes consistently altered in both experimental comparisons but not in the control comparison (Supplementary Data 7). Among these 87, only one was localized to the *Cctq1a* critical region, *Ctsc*, which was modestly (-0.8 $\log_2$ fold) but consistently and significantly ($p = 5 \times 10^{-5}$; $Q =$ 0.0009) down regulated in comparing the SJL allele to the KS allele. Web Gestalt[21] was used for over-representation analysis comparing the list of 87 differentially expressed genes to a background list of all genes expressed in the cornea with a FPKM ≥ 1 in any strain. Results of the analysis indicate a strong signal for several collagen-related categories (fibrillar collagen trimer, abnormal cutaneous collagen fibril morphology, collagen biosynthesis and modifying

enzymes, collagen degradation, etc.), extracellular-matrix-related categories (extracellular matrix component, ECM proteoglycans, degradation of the extracellular matrix, etc.) and ocular-related categories (decreased corneal stroma thickness, abnormal corneal epithelium morphology, abnormal cornea morphology, and abnormal eye morphology) (Supplementary Data 8).

Functional tests of lead candidates

Based on candidate prioritization criteria, *Fzd4* and *Ctsc* were initially considered the top candidates. To test the influence of *Fzd4* on CCT, we tested a strain with a targeted mutation of *Fzd4* (B6;129-*Fzd4*^{tm1Nat}/J) on a segregating B6 and 129 background[22]. *Fzd4*^{tm1Nat} homozygotes had a chocolate coat color not expected from either background. This observation is meaningful as the gene responsible for this phenotype, *Rab38*, is physically near *Fzd4* and within the *Cctq1* critical region, i.e., the strain is likely a double mutant for *Fzd4* (genotype verified) and *Rab38* (mutation unknown). However, there was no correlation between *Fzd4* ^{tm1Nat} genotype and CCT (p = 0.819; one-way ANOVA comparing all three genotypes among littermates; Figure 3B; Supplementary Data 3–5). In genetic complementation crosses, *Fzd4* ^{tm1Nat} mutation complemented the congenic interval ([*Fzd4*^{WT}/*Cctq1a*^{SJL} F1] vs. [*Fzd4*^{HET}/*Cctq1a*^{SJL} F1]; p = 0.528; Student's two-tailed t-test; n = 4-6 per genotype; Figure 3C; Supplementary Data 3–5). The complementation cross also highlighted the coat color phenotype associated with the *Fzd4*^{tm1Nat} mutation, with *Fzd4*^{WT}/*Cctq1a*^{SJL} F1 mice (*Tyr*^{HET}) having a black coat color with normally pigmented eyes and *Fzd4*^{HET}/*Cctq1a*^{SJL} F1 mice (*Tyr*^{HET}) having an unmistakable lightened ("light chocolate") coat color and light brown irides instead of brown (Supplementary Data 9). Therefore, *Fzd4* was ruled out as causative of the *Cctq1a* phenotype, and *Rab38* further deprioritized as a candidate.

To test the influence of *Ctsc* on CCT, we imported a strain with a targeted mutation of *Ctsc* (B6.Cg-*Ctsc*^{tm1Ley}) on an N10 congenic B6 background[23]. Because the targeted mutation was generated on an albino 129 background, and *Ctsc* is physically linked to *Tyr*, *Ctsc*^{tm1Ley} homozygotes are albino, i.e., the strain is a double mutant for *Ctsc* and *Tyr*. This is meaningful because the SJL/J strain is albino and the *Tyr*^{c} mutation is within the KS.SJL-*Cctq1a* congenic interval. Homozygotes had a statistically significant decrease in CCT compared to littermate controls ($p < 0.002$ for albino *Ctsc*^{tm1Ley} vs. pigmented *Ctsc*^{HET}; $p < 0.002$ for albino *Ctsc*^{tm1Ley} vs. pigmented *Ctsc*^{WT}; one-way ANOVA with Tukey post-test comparing all three genotypes among littermates; n=10–12 mice per genotype; Figure 3D; Supplementary Data 3–5). In genetic complementation crosses, *Ctsc*^{tm1Ley} failed to complement *Cctq1a*^{SJL} ($p < 0.001$ for pigmented [*Ctsc*^{tm1Ley}/*Cctq1a*^{KS} F1] vs. albino [*Ctsc*^{tm1Ley}/*Cctq1a*^{SJL} F1]; Student's two-tailed t-test; n = 10–11 mice per genotype; Figure 3E; Supplementary Data 3–5). Therefore, *Ctsc or Tyr* were determined to be causative of the *Cctq1a* phenotype.

To differentiate *Ctsc* and *Tyr* as the causative mutation, independent alleles on a pure B6 background were assessed. To test *Ctsc*, four new mutations predicted to result in null protein were generated in B6 mice with CRISPR-Cas9 technology (Supplementary Data 10). To test *Tyr*, a well-known spontaneous mutation that was commercially available, *Tyr*$^{c-2J}$, was analyzed[24, 25]. There was no association between *Ctsc*^{KO} genotype and CCT ($p = 0.237$; one-way ANOVA comparing all three genotypes among littermates; n = 9–17 mice per group; Figure 3F; Supplementary Data 3-5). In genetic complementation crosses with the congenic strain, the *Ctsc*^{tm1Mga} mutation (46bp-deletion in the coding sequence of exon 1 leading to no detectable CTSC protein; Supplementary Data 10) complemented the congenic phenotype ($p = 0.696$; Student's two-tailed t-test; n = 8–12 mice per group; Figure 3G; Supplementary Data 3–5). In contrast, albino *Tyr*$^{c-2J}$ mice had decreased CCT relative to pigmented B6 ($p < 0.001$; Student's two-tailed t-test; n = 9–10 mice per group; Figure 3H; Supplementary Data 3–5). In genetic

complementation crosses with the congenic strain, the *Tyr*$^{c\text{-}2J}$ mutation failed to complement the congenic phenotype ($p < 0.001$ for pigmented [*Cctq1a*^{KS}/*Tyr*$^{c\text{-}2J}$ F1] vs. albino [*Cctq1a*^{SJL}/*Tyr*$^{c\text{-}2J}$ F1]; Student's two-tailed *t*-test; $n = 8$ mice per genotype; Figure 3I; Supplementary Data 3–5). Thus, only *Tyr* mutation was left as a feasible candidate for *Cctq1a*.

CRISPR-Cas9 technology was also used to generate new *Tyr* mutations on a C57BL/6J background (Supplementary Data 11). One allele was selected for propagation, *Tyr*^{tm4Mga}, an albinism-causing 4bp-deletion in the coding sequence of exon 1 that is predicted to cause a frameshift leading to a premature stop codon and RNA-mediated decay; i.e., a presumed null mutation. *Tyr*^{tm4Mga} mice had a significantly thinner cornea than littermate controls ($p < 0.002$ for *Tyr*^{WT} vs. *Tyr*^{tm4Mga}; $p < 0.002$ for *Tyr*^{HET} vs. *Tyr*^{tm4Mga}; one-way ANOVA with Tukey post-test comparing all three genotypes among littermates; $n = 6$–10 mice per genotype; Figure 4; Supplementary Data 5 and 12). Thus, a presumed null allele of *Tyr* caused the same albinism and thinning of CCT as found for the *c* and *c-2J* alleles.

Mechanism of *Tyr* function on CCT

In considering the possible mechanism through which *Tyr* might influence CCT, three hypotheses were tested:

The first candidate mechanism centered on the role of DOPA, which is a cofactor in the oxidation of tyrosine by TYR, leading to melanin production[26], and a substrate for tyrosine hydroxylase (TH), leading to dopamine synthesis. Dopamine is considered a key molecule in ocular growth[27, 28], and mice with a conditional knock-out of *Th* in the retina have previously been shown to have decreased CCT[29]. Rationalizing that some DOPA may normally escape from pigment producing cells to influence CCT via a TH-dependent mechanism, we tested whether providing supplemental DOPA in the drinking water of albino mice would rescue the

decreased CCT associated with albinism. No statistically significant effect was observed (Figure 5; Supplementary Data 5), discounting the hypothesis that a DOPA deficit was rate-limiting for CCT determination in *Tyr* mutant mice.

The second candidate mechanism revolves around the possibility of a gene-environment interaction involving temperature and light. In this series of experiments, mice were reared in environmental control chambers in combinations of different temperatures and light cycles. Cohorts included pigmented B6, albino $Tyr^{c\text{-}2J}$, and the temperature sensitive himalayan mutation (B6.Cg-$Tyr^{c\text{-}h}$/J)[30, 31]. At ambient temperatures, $Tyr^{c\text{-}h}$ homozygotes are only partially pigmented on the coolest parts of the body (such as the ears, nose, tail, and eyes) and CCT is intermediate between B6 and $Tyr^{c\text{-}2J}$ mice (Supplementary Data 5, 13, and 14). For CCT of mice raised at ambient temperature, genetic complementation tests again confirmed the influence of *Tyr*-mediated albinism on CCT ($p = 0.337$ for [pigmented B6 x $Tyr^{c\text{-}h}$ F1] vs. [pigmented B6 x $Tyr^{c\text{-}2J}$ F1]; $p < 0.002$ for [pigmented B6 x $Tyr^{c\text{-}h}$ F1] vs. [albino $Tyr^{c\text{-}h}$ x $Tyr^{c\text{-}2J}$ F1]; and $p < 0.002$ for [pigmented B6 x $Tyr^{c\text{-}2J}$ F1] vs. [albino $Tyr^{c\text{-}h}$ x $Tyr^{c\text{-}2J}$ F1]; one-way ANOVA with Tukey post-test; $n = 4–14$ mice per group, Supplementary Data 5). At decreased temperatures $Tyr^{c\text{-}h}$ homozygotes can generate pigment more broadly, and at increased temperatures the albinism is accentuated (Supplementary Data 13 and 14).

Regarding temperature, comparison of B6.$Tyr^{c\text{-}h}$ mice, as well as B6 and B6.$Tyr^{c\text{-}2J}$ controls, raised at 10°C vs. 32°C in environmental control chambers with a standard light cycle, showed that CCT followed pigment status; the thin CCT of hypopigmented $Tyr^{c\text{-}h}$ mice reared at increased temperature (i.e., lower TYR activity) was rescued by rearing the $Tyr^{c\text{-}h}$ mice at decreased temperature (i.e., higher TYR activity; $Tyr^{c\text{-}h}$ at 32°C vs. $Tyr^{c\text{-}h}$ at 10°C; Δ 10.9 µm; $p < 0.001$; $n = 13–15$ mice per condition; one-way ANOVA with Sidak test; Figure 6; Supplementary Data 5). In testing the effect of temperature on corneal thickness in controls,

there was a small (Δ 2.8 µm) and nominally significant (p = 0.03) decreased CCT in mice raised at 10ºC compared to mice raised at 32ºC when considering all C57BL/6J and *Tyr*$^{c\text{-}2J}$ mice across the experiment (n = 16 mice vs. n = 19 mice, Type II ANOVA) and there was no interaction between genotype and temperature. In sum, changing environmental temperature changed CCT of the *Tyr*$^{c\text{-}h}$ mice as predicted.

Regarding light, comparison of B6.*Tyr*$^{c\text{-}h}$ mice, as well as B6 and B6.*Tyr*$^{c\text{-}2J}$ controls, raised at 10°C vs. 32°C in environmental control chambers with dark-rearing of mice from conception to 10–15 weeks of age rescued the thin CCT phenotype associated with albinism (p < 0.001 for [*Tyr*$^{c\text{-}h}$ at 32°C standard light] vs. [*Tyr*$^{c\text{-}h}$ at 32°C dark rear]; p < 0.03 for [*Tyr*$^{c\text{-}2J}$ at 10°C standard light vs. *Tyr*$^{c\text{-}2J}$ at 10°C dark rear]; p < 0.001 for [*Tyr*$^{c\text{-}2J}$ at 32°C standard light vs. *Tyr*$^{c\text{-}2J}$ at 32°C dark rear]; n = 5–16 per condition; one-way ANOVA with Sidak test; Figure 6; Supplementary Data 5). Rearing pigmented B6 mice in constant light is known to lead to an increase in axial length[32]. OCT examinations of independent cohorts of C57BL/6J and *Tyr*$^{c\text{-}2J}$ mice for the purpose of measuring axial length show that *Tyr*$^{c\text{-}2J}$ mice have a 65.6 µm greater axial length on average compared to C57BL/6J mice (3.453 mm vs. 3.388 mm, respectively; p < 0.001, Student's two-tailed t-test; n = 10 male and 10 female mice per strain; Figure 7).

Discussion

Using a phenotype-driven quantitative genetic analysis of CCT, physical mapping led to identification of a small critical region containing 10 genes, of which we ruled out three (*Fzd4*, *Rab38*, *Ctsc*) and found via an analysis of a *Tyr* allelic series (*c*, *c-2J*, *c-h*) that *Tyr* is the causative gene underlying the *Cctq1a* QTL. *Tyr* is by no means an unknown gene—it was in fact one of the first known mammalian genes whose initial discovery predates the word "gene"[26, 33, 34]. However, *Tyr* was a surprising gene to find linked to CCT. TYR is an oxidase whose only known biological role relates to melanin synthesis[26, 35]. Although there are small numbers of

pigmented cells in the corneal limbus, the cornea is by and large not only non-pigmented, but transparent. Furthermore, previously published data indicate that *Tyr* is not even expressed in the adult cornea[17], which is consistent with the current study which also found near-zero expression in the cornea at 3 weeks of age (RNA-Seq max expression ~1.3 FPKM; Supplementary Data 7). Thus, there is no molecular rationale for proposing that TYR has a direct function in corneal cells. If not for the current experiments, there would also be sparse biological rationales for proposing that TYR might influence corneal anatomy through any mechanism. Regardless, the current agnostic QTL study led to the conclusion that *Tyr* contributes to the primary genetic influence on CCT, at least in the context of KS x SJL hybrids. Experiments using multiple alleles on matched genetic backgrounds, in isolation and genetic complementation crosses, conclusively confirmed allelism of *Tyr-Cctq1a*; albino mice lacking TYR function have thin corneas. Rationalizing that albinism would expose the developing eye to increased light, one of the mechanistic experiments performed here compared the effect of dark-rearing on the CCT of albino vs. pigmented C57BL/6J mice. The results showed that the thin CCT phenotype of albino B6.$Tyr^{c\text{-}h}$ mice raised at 32°C and B6.$Tyr^{c\text{-}2J}$ mice was rescued by dark-rearing. Thus, we are led to propose an epiphenomenon, whereby developmental light exposure interacts with genotype as an important determinate of corneal thickness.

All current CCT measurements were done with mice 10–15 weeks of age, which is slightly past the age at which the cornea of B6 mice reaches its final adult thickness (~P55)[36]. Transcriptomic changes in the cornea related to *Tyr* genotype were detectable at 3 weeks of age. Thus, the timeframe for when *Tyr* can impact the cornea is presumably during anterior chamber development at some point preceding 3 weeks of age. Two mechanisms, which are both conjectural, might feasibly contribute to this early acting phenomenon. 1) Corneal development might be a component of refractive development. Emmetropization typically occurs in the first months following eyelid opening, with impacts from both the amount of light and its focus on the

retina[32,37]. Thus, it is feasible that albinism could in effect cause blur (from light not being absorbed by melanin and reflecting within the eye), which induces relative myopia and CCT thinning with rearing in normal lights, but not in dark-rearing. 2) Corneal development might be influenced by central or corneal circadian outputs. Circadian outputs arise from both central and peripheral clocks, with the suprachiasmatic nucleus (SCN) being a central master pacemaker that receives light signals from retinal ganglion cells and subsequently coordinates phasing to peripheral tissues[38, 39]. Notably, the SCN receives retinal input from the retinohypothalamic tract, which is known to be expanded in albinos[40, 41, 42]. Thus, one possibility is that factors increasing SCN output (such as albinism or cycling light conditions) might lead to decreased CCT and those decreasing the signaling (such as dark rearing) might lead to increased CCT. Refractive and circadian mechanisms could also be acting in an intertwined way[43]. Additional experiments are needed to distinguish these, and possibly other, mechanisms relevant to our current findings.

A leading candidate for contributing to the molecular mechanism causing thin CCT in albino mice was DOPA, which is a cofactor for TYR[26, 35], a substrate for TH leading to dopamine (reviewed in [27]), and an endogenous ligand for the G-protein-coupled receptor GPR143[44] . DOPA can modulate refractive development[27, 29, 40] and the circadian system[45], as well development of multiple ocular tissues[46, 47]. Notably, mice with a conditional knock-out of *Th* in the retina have decreased CCT[29]. The current experiments with *Tyr* mutant mice were not able to detect a role for DOPA in influencing CCT of these albino strains, though an important caveat to point out is that only a single dosing schedule for DOPA supplementation was currently tested.

It is unclear whether albinism or pigmentation influences CCT in humans, though our current experiments suggest this is likely. In humans, loss of function mutations in *TYR* cause

oculocutaneous albinism type 1 (OCA 1)[35, 48]. It's unclear from the literature if humans with OCA 1 have decreased CCT; it may be difficult to ascertain because of relatively small patient populations and confounding variables such as eye rubbing[49].

The current study has several implications with respect to mouse genetics and mouse models of disease: 1) The results highlight the potential for environmental influences on ocular development, which have been quantitated here for CCT, but may extend to other tissues as well. 2) The results indicate that albino mice should be tested for potentially being a naturally occurring model of myopia. 3) Because CCT is a complex trait, there is little reason to suspect that different inbred albino mouse strains would necessarily have the thinnest CCT in comparison to other inbred strains that are pigmented[50], only that they would have thinner CCT as albino mice compared to pigmented mice *within* an inbred strain. However, for any experiment using such an albino strain, or cohorts in which an allele such as the common Tyr^{c} allele is segregating, attention to the possibility of environmental influences is warranted. 4) *Tyr* has been linked with many ophthalmic traits in mice[40, 41, 42, 46, 51, 52, 53, 54, 55, 56]; in some instances, a consideration of gene-environment interactions in the mechanism of these various models may be warranted. And finally, 5) our study uncovers a genetic peculiarity. *Cctq1* was originally reported as a single QTL on chromosome 7, detected in an F2 intercross of KS and SJL inbred mice[16]. In studies of successive generations of congenic mice, N4F2 mice heterozygous for the *Cctq1* alleles showed the original differential phenotype (over-dominant, *increased* CCT compared to littermate controls)[16], whereas in N10–N15 intercrosses, mice homozygous for the SJL allele showed the differential phenotype (recessive, *decreased* CCT compared to littermate controls). As the sub-congenics were intercrossed and analyzed for CCT, KS.SJL-$Cctq1a^{SJL};Cctq1b^{KS}$ mice consistently had thinner corneas than KS.SJL-$Cctq1a^{KS};Cctq1b^{KS}$ mice of the same generation, but there were also fluctuations in absolute value related to generation and interval size. The likely explanation for these observations is that there was

more than one CCT-modifying gene in the original *Cctq1* interval, which was in fact found to be the case by the resolution of *Cctq1* into *Cctq1a* and *Cctq1b*. This is consistent with the findings of human GWAS, indicating that there are likely hundreds of CCT-influencing genes dispersed throughout the genome, many of which will be physically close to one another. In mice, it is known that as a locus is narrowed using congenics, genes can be segregated away from nearby modifiers and the overall phenotype of the original QTL can be reduced, disappear, or reverse its apparent effect[57, 58]. The current data seem to exemplify this phenomenon.

In summary, our phenotype-driven genetic study of CCT identified *Tyr* as a significant regulator of CCT in mice. The molecular findings of this study were unexpected. We propose that the results can be explained by an epiphenomenon whereby a gene:environment interaction; i.e., *Tyr*-mediated albinism allowing increased exposure of the eye to light has an important influence on corneal development.

Materials and Methods

Experimental animals

All animals were treated in accordance with the ARVO Statement for the Use of Animals in Ophthalmic and Vision Research. The majority of mice were housed and bred at the University of Iowa Research Animal Facility with approval for experimental protocols conferred by the Institutional Animal Care and Use Committee of the University of Iowa. Two cohorts of mice, the C57BL/6J (JAX Stock No. 000664) and B6.Cg-*Tyr*$^{c\text{-}2J}$/J (JAX Stock No. 000058) used for in vivo axial length measurements (Figure 7) were purchased from The Jackson Laboratory at 10-weeks-old and subsequently housed at the University of California San Francisco until 12-weeks-old with approval for experimental protocols conferred by the Institutional Animal Care and use Committee at the University of California San Francisco. Mouse strains used in this

study include: SJL/J (Stock No. 000686), C57BLKS/J (JAX Stock No. 000662), C57BL/6J (JAX Stock No. 000664), B6.Cg-*Tyr*$^{c\text{-}2J}$/J (JAX Stock No. 000058), B6;129-*Fzd4*^{tm1Nat}/J (JAX Stock No. 012823), B6.Cg-*Tyr*$^{c\text{-}h}$/J (JAX Stock No. 000104; Imported from Dr. Brian Brooks at the NIH), B6.Cg-*Ctsc*^{tm1Ley} (Imported from Dr. Christine Pham at Washington University), KS.Cg-SJL^{Cctq1}, B6-*Ctsc*^{tm1Mga}, and B6-*Tyr*^{tm4Mga}. All experiments included male and female mice.

Chromosome 7 QTL analysis

The chromosome 7 quantitative trait locus analysis was performed with R/qtl, using the two-dimensional genome-wide scan (scantwo). Significance thresholds were determined empirically by permutation testing, using 1000 permutations. The validity of a multiple QTL model was tested by performing a multiple regression analysis. Phenotypic variance was estimated and the full model was statistically compared to reduced models in which one QTL was dropped.

Constructing congenic mice

A ~38.3cM genomic region (*i.e.*, *Cctq1*) spanning from *D7Mit318* (SSLP marker at 42.3 cM) to *rs13479545* (SNP marker at 81.2 cM) was transferred from SJL/J mice (abbreviated throughout as SJL; thick cornea) onto the genetic background of C57BLKS/J mice (abbreviated throughout as KS; thin cornea) by reiterative backcrossing. Mice carrying the SJL alleles within the region (*i.e.*, KS.SJL-*Cctq1*^{Het}) were selected at each generation by using a panel of six markers that were tested and found to be polymorphic between KS and SJL mice. At the N10 generation, mice were intercrossed. At this point, *Cctq1* was treated as a digenic locus, renamed to *Cctq1a* and *Cctq1b* (see Results and Figure 2). *Cctq1a* encompassed the region spanning from *D7Mit318* (42.3 cM) to *D7Mit220* (55.7 cM). *Cctq1b* spanned from *D7Mit105* (70.3 cM) to *rs13479545* (81.2 cM). All genotype combinations of *Cctq1a* and *Cctq1b* (9 possible combinations; *i.e.*, homozygosity for KS alleles, heterozygous, or homozygosity for SJL alleles at each locus) were analyzed for their effect on CCT.

Sub-congenic mice harboring reduced *Cctq1a* intervals (KS alleles at *Cctq1b*) were also generated. At N12, *Cctq1a* was reduced to a 15.9 cM region spanning from *D7mit347* to *D7mit321*. These N12 sub-congenic mice are referred to throughout as KS.SJL-*Cctq1a*(15.9cM). At N15, *Cctq1a* was reduced to a 9.9 cM region spanning from *rs3672782* to *D7mit321*. These sub-congenic N15 mice are referred to throughout as KS.SJL-*Cctq1a*(9.9cM). Sub-congenic mice were intercrossed, and all genotypes were assessed for the CCT phenotype. The KS.SJL-*Cctq1* line has been sperm cryopreserved.

CCT phenotyping

All measurements were recorded from adult mice. Mice were injected with a standard mixture of ketamine/xylazine (intraperitoneal injection of 100 mg ketamine + 10 mg xylazine / kg body weight; Ketaset®, Fort Dodge Animal Health, Fort Dodge, IA; AnaSed®, Lloyd Laboratories, Shenandoah, IA). During induction of anesthesia, mice were provided supplemental indirect warmth by a heating pad. Immediately following anesthesia, eyes were hydrated with balanced salt solution (BSS; Alcon Laboratories, Fort Worth, TX) and corneal images were obtained with a Bioptigen optical coherence tomographer (SD-OCT; Bioptigen, Inc., USA). A 12mm telecentric bore with a reference arm position of 1048 was used to image the anterior segment of each eye. The bore was positioned such that the pupil of the eye was centered in the volume intensity projection. Scan parameters were as follows: radial volume scans 2.0 mm in diameter, 1000 A-scans/B-scan, 100 B-scans/volume, 1 frame/B-scan, and 1 volume. Central corneal thickness (CCT) was measured for each eye using vertical angle-locked B-scan calipers. Mice were included in the analysis if the difference between the right and left eyes was less than 7 µm and if both eyes were free from opacity. The average CCT and standard deviation for each genotype was statistically compared using Student's two-tailed *t*-test for comparison of two cohorts or one-way ANOVA with a Tukey post-test for comparison of three or more cohorts.

Recombination mapping

For genetic mapping of the gene underlying *Cctq1a*, additional polymorphic markers were identified and tiled into the region. Intercrosses of N10 mice were continued and mice with informative recombination events were analyzed for the CCT phenotype. Based on the allelic effects of the QTL on the CCT phenotype (see Results), the genomic boundaries of the QTL (and hence, the region of the underlying gene) were deduced by comparing the phenotype of the recombinant mice with the location of the recombination event within the critical interval. The following is a complete list of all the polymorphic markers used for genotyping (listed in order from centromeric to telomeric): *D7Mit318*, *rs13479346*, *rs13479362*, *D7Mit347*, *D7Mit62*, *rs6271685*, *rs108403472*, *Cctq1a-STR5*, *D7Mit31*, *rs3672782*, *rs32438580*, *rs3663323*, *rs13479392*, *rs13479393*, *rs6247100*, *rs13479395*, *D7Mit301*, *D7Mit321*, *D7Mit220*, *D7Mit238*, *D7Mit105*, *rs13479535*, *rs13479536*, and *rs13479545*. Primer sequences are available upon request.

Exome sequence analysis

High quality genomic DNA was harvested from KS and SJL spleen tissue using a Qiagen DNeasy Blood and Tissue kit following the manufacturer's instructions; an RNA digestion step was included. DNA samples were sent to BGI Americas for sequencing and passed their quality control standards. Libraries were constructed with an Agilent SureSelect 50Mb Mouse Exome Capture Kit and were sequenced with 50X coverage using an Illumina HiSeq2000. Standard bioinformatics analysis was conducted in which the data was filtered (by removing adaptor contamination and low-quality reads from raw reads), aligned, and SNPs were called and annotated using a reference genome (GRCm38 build).

RNASeq analysis

N12F3 KS.SJL-*Cctq1a(15.9cM)*^{KS}, KS.SJL-*Cctq1a(15.9cM)*^{SJL}, and KS inbred mice were euthanized at three weeks of age by cervical dislocation. Immediately upon death, mice were enucleated, and the eyes were placed in RNase free dishes (NEST Biotechnology) containing RNA*later* RNA stabilization reagent. Corneas from mice were dissected in RNA*later* and pooled to make one sample (6 corneas per sample); three samples were collected per genotype. Cornea samples were either stored at -80^{o}C in RNA*later* or processed immediately. Corneas were transferred from RNA*later* to 0.7 mL of lysis/binding buffer from the *mir*Vana miRNA isolation kit (Ambion) and homogenized for 1 minute using a tissue tearer (Biospec Products, Inc.). The homogenate was then passed through a QIAshredder column (Qiagen) and the lysate was collected. For the remainder of the procedure, the samples were processed using the *mir*Vana kit for total RNA according to the manufacturer's instructions. The quality and concentration of the RNA was analyzed using a NanoDrop 2000 and the Agilent Model 2100 Bioanalyzer. All samples had RNA integrity numbers of 9.5 or greater, indicating high quality RNA with little degradation of the samples. Samples were barcoded and stranded libraries were prepared by the Genomics Division of the Iowa Institute of Human Genetics. The nine libraries were pooled together, split into two equal parts, and run on two lanes of an Illumina HiSeq to obtain 100 base pair, paired-end sequence reads.

Reads were mapped to the mm10 mouse genome build using Tophat2 (ver 2.0.11; [PMID: 23618408]). The '-r' parameter was set to 135, and the '--no-coverage-search' option was used. Transcript abundance was quantified using Cufflinks (ver. 2.1.1; [PMID: PMC3146043]) for RefSeq transcript models from the Illumina iGenomes mm10 package. Ribosomal RNA and mitochondrial gene loci, obtained from USCS Genome Table Viewer, were masked from the Cufflinks analysis, and the '--max-bundle-frags' parameter was set to 20000000. Differential expression between genotypes was performed using Cuffdiff (ver. 2.1.1; [PMID: 23222703]). Genes identified from each comparison were subsequently filtered for only those with a q-value

≤ 0.001 and a mean FPKM (Fragments Per Kilobase of transcript per Million mapped reads) value ≥ 1 in at least one of the strains. Functional enrichment analysis was performed with WebGestalt [32, 33] with analysis parameters detailed in Supplementary Data 8.

Constructing *Ctsc* null mice

B6-*Ctsc*^{KO} mice were generated by the Genome Editing Facility at The University of Iowa on a pure C57BL/6J (JAX Stock No. 000664) background by targeting *Ctsc* Exon 1 with CRISPR/Cas9 using guide sequence: CGTGCGCTCCGACACTCCTGCC. Founders were crossed with C57BL/6J mice and offspring analyzed for germline transmission of *Ctsc* mutations. From four founders, we observed transmission of four separate *Ctsc* mutations, all predicted to be null based on Sanger sequencing results. Three *Ctsc* mutations were propagated in separate intercross mouse lines and were validated as null mutations by Western Blot using an antibody against CTSC (Catalog #AF1034; R&D Systems, Inc.; Minneapolis, MN; Supplementary Data 10). One of these mutations, *Ctsc*^{tm1Mga}, is a 46 bp exon 1 coding sequence deletion that was used for additional downstream analysis.

Constructing *Tyr* null mice

To generate mice with *Tyr* null mutations on a pure C57BL/6J (JAX Stock No. 000664) background, the Genome Editing Facility at the University of Iowa targeted *Tyr* Exon 1 with CRISPR/Cas9 using two guide sequences simultaneously: 1) CCATGGATGGGTGATGGGAG and 2) TTCAAAGGGGTGGATGACCG. Founders were crossed with C57BL/6J mice and offspring analyzed by Sanger sequencing for germline transmission of *Tyr* mutations. This experiment generated more alleles than we could reasonably work with (15 unique mutations identified via sequencing; Supplementary Data 12). For each unique mutation, we set up a complementation cross with B6.*Tyr*$^{c-2J}$ and screened progeny coat color for alleles conferring novel function. F1 progeny were screened for 14 alleles; the mice harboring the remaining allele

did not produce F1 progeny. All 14 alleles produced a standard albino coat color in trans with the *Tyr*$^{c\text{-}2J}$ mutation, indicating failure to complement. Going forward, we chose to complete additional studies for one allele, *Tyr*^{tm4Mga}, which is a 4 bp deletion in the coding sequence of exon 1, causes a frameshift and leads to a premature stop codon predicted to cause RNA-mediated decay (i.e., a presumed null mutation). Accordingly, homozygotes of this strain are albino.

L-DOPA supplementation studies

Breeder cages of C57BL/6J, B6.Cg-*Tyr*$^{c\text{-}2J}$/J, and B6.Cg-*Tyr*$^{c\text{-}h}$/J were provided with water bottles containing water only (control) or water with 200mg/L of L-DOPA, with 30mg/L of benserazide to minimize the conversion of L-DOPA to dopamine in the peripheral nervous system. Fresh water bottles were prepared and supplied every Monday, Wednesday, and Friday. Litters were weaned into cages where they continued to receive the same treatment of supplemented water until 13–16 weeks old.

Environmental chamber

Breeder cages of C57BL/6J, B6.Cg-*Tyr*$^{c\text{-}2J}$/J, and B6.Cg-*Tyr*$^{c\text{-}h}$/J were housed in rodent environmental control chambers (Powers Scientific) either at 10°C or 32°C and with either a standard light cycle (12 hrs on/12 hrs off) or dark-rearing. Resulting pups were born and group-housed at the altered temperature and light cycle until adulthood, when CCT was analyzed by OCT at 10–15 weeks old.

Axial length phenotyping

Envisu R4300 spectral-domain optical coherence tomography (SD-OCT, Leica/Bioptigen Inc., Research Triangle Park, NC, USA) was employed to measure the ocular axial length in adult

(12-week-old) mice[59]. Mice were anesthetized with ketamine/xylazine (100 mg/kg and 5mg/kg, respectively; intraperitoneal) and their eyes dilated before placing the animal in a cylindrical holder. The eye was hydrated with Genteal (Alcon, Fort Worth, TX, USA) and positioned in front of the OCT light source. Correct alignment of the eye was achieved by placing the Purkinje image in the center of the pupil. The images were acquired in rectangular volume and radial volume scans. The axial length was calculated by measuring the distance from the corneal surface to the RPE/choroid interface for both the left and right eyes of a given mouse. Measurements from the left and right eye of each mouse were averaged to give a single measurement per animal. Measurements from all eyes were included in the analysis. To minimize the possible effect of body weight on ocular size, we ensured that body weight of littermates was within a narrow range in each of the comparative groups. The average axial length and standard deviation for each genotype was statistically compared using Student's two-tailed *t*-test.

Statistics

A multiple regression analysis, in which each locus and the interaction component were sequentially dropped from the 2-QTL model, was used to analyze the presence of two interacting loci on chromosome 7. Student's two-tailed *t*-test was used to evaluate the difference between two independent genotypes for CCT (*t*-values and degrees of freedom for each comparison are listed in Supplementary Data 5) and axial length (*t*-value = 5.415; degrees of freedom = 38). A one-way ANOVA with a Tukey post-test was used to evaluate the difference between three or more independent genotypes for CCT (*f*-values and degrees of freedom for each comparison are listed in Supplementary Data 5). A one-way ANOVA with Sidak test was used to evaluate four comparisons to determine the effect of two environmental conditions on CCT in B6.cg-*Tyr*$^{c\text{-}h}$ and B6.cg-*Tyr*$^{c\text{-}2J}$ mice (f-value and degrees of freedom are listed in Supplementary Data 5).

ACKNOWLEDGEMENTS

The authors would like to thank Karl Broman for analyzing chromosome 7 of our original F2 dataset with us. Transgenic mice were generated at the University of Iowa Genome Editing Core Facility directed by William Paradee, PhD and supported in part by grants from the NIH and from the Roy J. and Lucille A. Carver College of Medicine. We wish to thank Norma Sinclair, Patricia Yarolem and Joanne Schwarting for their technical expertise in generating transgenic mice.

The authors declare no competing interests.

AUTHOR CONTRIBUTIONS

K.J.M., D.R.L., and M.G.A. conceived and designed the experiments. K.J.M., D.R.L., C.J.V., A.H.B., L.M.D., N.P., H.E.M., M.N.A., and M.G.A. performed the experimental work. K.J.M., D.R.L., and M.G.A. performed experimental data analysis and interpreted the results with contributions from all authors. S.S.W. analyzed the RNA-seq data supervised by T.E.S. W.J.P. constructed the transgenic mice. S.K. performed the axial length experiment supervised by K.S.N. K.W. verified and performed statistical analyses. K.J.M., D.R.L. and M.G.A. wrote the manuscript with input from all authors. M.G.A. supervised the study and provided funding.

REFERENCES

1. Pediatric Eye Disease Investigator G, *et al.* Central corneal thickness in children. *Arch Ophthalmol* **129**, 1132-1138 (2011).

2. Hashmani N, *et al.* Effect of age, sex, and refractive errors on central corneal thickness measured by Oculus Pentacam((R)). *Clin Ophthalmol* **11**, 1233-1238 (2017).

3. Tayyab A, Masrur A, Afzal F, Iqbal F, Naseem K. Central Corneal Thickness and its Relationship to Intra-Ocular and Epidmiological Determinants. *J Coll Physicians Surg Pak* **26**, 494-497 (2016).

4. Brandt JD, Beiser JA, Kass MA, Gordon MO, Ocular Hypertension Treatment Study G. Central Corneal Thickness in the Ocular Hypertension Treatment Study (OHTS). *Ophthalmology* **127**, S72-S81 (2020).

5. La Rosa FA, Gross RL, Orengo-Nania S. Central corneal thickness of Caucasians and African Americans in glaucomatous and nonglaucomatous populations. *Arch Ophthalmol* **119**, 23-27 (2001).

6. Swierkowska J, Gajecka M. Genetic factors influencing the reduction of central corneal thickness in disorders affecting the eye. *Ophthalmic Genet* **38**, 501-510 (2017).

7. Toh T, *et al.* Central corneal thickness is highly heritable: the twin eye studies. *Investigative ophthalmology & visual science* **46**, 3718-3722 (2005).

8. Zheng Y, *et al.* Heritability of central corneal thickness in Chinese: the Guangzhou Twin Eye Study. *Investigative ophthalmology & visual science* **49**, 4303-4307 (2008).

9. Choquet H, *et al.* A multiethnic genome-wide analysis of 44,039 individuals identifies 41 new loci associated with central corneal thickness. *Commun Biol* **3**, 301 (2020).

10. Iglesias AI, *et al.* Cross-ancestry genome-wide association analysis of corneal thickness strengthens link between complex and Mendelian eye diseases. *Nat Commun* **9**, 1864 (2018).

11. Dhooge T, *et al.* More than meets the eye: Expanding and reviewing the clinical and mutational spectrum of brittle cornea syndrome. *Hum Mutat,* (2021).

12. Lu Y, *et al.* Genome-wide association analyses identify multiple loci associated with central corneal thickness and keratoconus. *Nature genetics* **45**, 155-163 (2013).

13. Lu Y, *et al.* Common genetic variants near the Brittle Cornea Syndrome locus ZNF469 influence the blinding disease risk factor central corneal thickness. *PLoS Genet* **6**, e1000947 (2010).

14. Dimasi DP, *et al.* Novel quantitative trait loci for central corneal thickness identified by candidate gene analysis of osteogenesis imperfecta genes. *Hum Genet* **127**, 33-44 (2010).

15. Zhang J, Wu D, Dai Y, Xu J. Functional relevance for central cornea thickness-associated genetic variants by using integrative analyses. *BioData Min* **11**, 19 (2018).

16. Lively GD, Koehn D, Hedberg-Buenz A, Wang K, Anderson MG. Quantitative trait loci associated with murine central corneal thickness. *Physiological genomics* **42**, 281-286 (2010).

17. Lively GD, *et al.* Genetic Dependence of Central Corneal Thickness among Inbred Strains of Mice. *Investigative ophthalmology & visual science* **51**, 160-171 (2010).

18. Broman KW, Sen S. *A Guide to QTL Mapping with R/qtl*. Springer Science+Business Media (2009).

19. Broman KW, Wu H, Sen S, Churchill GA. R/qtl: QTL mapping in experimental crosses. *Bioinformatics* **19**, 889-890 (2003).

20. Wynn EH, Sanchez-Andrade G, Carss KJ, Logan DW. Genomic variation in the vomeronasal receptor gene repertoires of inbred mice. *BMC Genomics* **13**, 415 (2012).

21. Liao Y, Wang J, Jaehnig EJ, Shi Z, Zhang B. WebGestalt 2019: gene set analysis toolkit with revamped UIs and APIs. *Nucleic acids research* **47**, W199-W205 (2019).

22. Wang Y, Huso D, Cahill H, Ryugo D, Nathans J. Progressive cerebellar, auditory, and esophageal dysfunction caused by targeted disruption of the frizzled-4 gene. *J Neurosci* **21**, 4761-4771 (2001).

23. Pham CT, Ley TJ. Dipeptidyl peptidase I is required for the processing and activation of granzymes A and B in vivo. *Proc Natl Acad Sci U S A* **96**, 8627-8632 (1999).

24. Le Fur N, Kelsall SR, Mintz B. Base substitution at different alternative splice donor sites of the tyrosinase gene in murine albinism. *Genomics* **37**, 245-248 (1996).

25. Green EL. Albino-2J (c<2J>). *Mouse News Lett* **49**, (1973).

26. Beermann F, Orlow SJ, Lamoreux ML. The Tyr (albino) locus of the laboratory mouse. *Mamm Genome* **15**, 749-758 (2004).

27. Zhou X, Pardue MT, Iuvone PM, Qu J. Dopamine signaling and myopia development: What are the key challenges. *Prog Retin Eye Res* **61**, 60-71 (2017).

28. Feldkaemper M, Schaeffel F. An updated view on the role of dopamine in myopia. *Exp Eye Res* **114**, 106-119 (2013).

29. Bergen MA, *et al.* Altered Refractive Development in Mice With Reduced Levels of Retinal Dopamine. *Investigative ophthalmology & visual science* **57**, 4412-4419 (2016).

30. Kidson S, Fabian B. Pigment synthesis in the Himalayan mouse. *J Exp Zool* **210**, 145-152 (1979).

31. Kwon BS, Halaban R, Chintamaneni C. Molecular basis of mouse Himalayan mutation. *Biochem Biophys Res Commun* **161**, 252-260 (1989).

32. Tkatchenko TV, *et al.* Photopic visual input is necessary for emmetropization in mice. *Exp Eye Res* **115**, 87-95 (2013).

33. Allen GM. The heredity of coat color in mice. *Proceedings of the American Academy of Arts and Sciences* **40**, 61-163 (1904).

34. Castle WE, Allen GM. The heredity of albinism. *Proceedings of the American Academy of Arts and Sciences* **38**, 603-622 (1903).

35. Seruggia D, Josa S, Fernandez A, Montoliu L. The structure and function of the mouse tyrosinase locus. *Pigment Cell Melanoma Res*, (2020).

36. Hanlon SD, Patel NB, Burns AR. Assessment of postnatal corneal development in the C57BL/6 mouse using spectral domain optical coherence tomography and microwave-assisted histology. *Exp Eye Res* **93**, 363-370 (2011).

37. Chakraborty R, Ostrin LA, Benavente-Perez A, Verkicharla PK. Optical mechanisms regulating emmetropisation and refractive errors: evidence from animal models. *Clin Exp Optom* **103**, 55-67 (2020).

38. Mohawk JA, Green CB, Takahashi JS. Central and peripheral circadian clocks in mammals. *Annu Rev Neurosci* **35**, 445-462 (2012).

39. Peirson SN, Brown LA, Pothecary CA, Benson LA, Fisk AS. Light and the laboratory mouse. *J Neurosci Methods* **300**, 26-36 (2018).

40. Steininger TL, Rye DB, Gilliland MA, Wainer BH, Benca RM. Differences in the retinohypothalamic tract in albino Lewis versus brown Norway rat strains. *Neuroscience* **54**, 11-14 (1993).

41. Miller AM, Chappell R, Obermeyer WH, Benca RM. Analysis of the retinohypothalamic tract in congenic albino and pigmented rats. *Brain Res* **741**, 348-351 (1996).

42. Fleming MD, Benca RM, Behan M. Retinal projections to the subcortical visual system in congenic albino and pigmented rats. *Neuroscience* **143**, 895-904 (2006).

43. Chakraborty R, Ostrin LA, Nickla DL, Iuvone PM, Pardue MT, Stone RA. Circadian rhythms, refractive development, and myopia. *Ophthalmic Physiol Opt* **38**, 217-245 (2018).

44. Lopez VM, Decatur CL, Stamer WD, Lynch RM, McKay BS. L-DOPA is an endogenous ligand for OA1. *PLoS Biol* **6**, e236 (2008).

45. Korshunov KS, Blakemore LJ, Trombley PQ. Dopamine: A Modulator of Circadian Rhythms in the Central Nervous System. *Front Cell Neurosci* **11**, 91 (2017).

46. Libby RT, *et al*. Modification of ocular defects in mouse developmental glaucoma models by tyrosinase. *Science* **299**, 1578-1581 (2003).

47. Lee H, Scott J, Griffiths H, Self JE, Lotery A. Oral levodopa rescues retinal morphology and visual function in a murine model of human albinism. *Pigment Cell Melanoma Res* **32**, 657-671 (2019).

48. Kirkwood BJ. Albinism and its implications with vision. *Insight* **34**, 13-16 (2009).

49. Rao VA, Swathi P, Chaitra, Thappa DM. Bilateral keratoconus with oculocutaneous albinism. *Indian J Dermatol Venereol Leprol* **74**, 407-409 (2008).

50. Dimasi DP, *et al*. Ethnic and mouse strain differences in central corneal thickness and association with pigmentation phenotype. *PLoS One* **6**, e22103 (2011).

51. Buttner C, *et al*. Tyrosinase Is a Novel Endogenous Regulator of Developmental and Inflammatory Lymphangiogenesis. *Am J Pathol* **189**, 440-448 (2019).

52. Mason C, Slavi N. Retinal Ganglion Cell Axon Wiring Establishing the Binocular Circuit. *Annu Rev Vis Sci* **6**, 215-236 (2020).

53. Savinova OV, *et al*. Intraocular pressure in genetically distinct mice: an update and strain survey. *BMC Genet* **2**, 12 (2001).

54. Johnson BA, Cole BS, Geisert EE, Ikeda S, Ikeda A. Tyrosinase is the modifier of retinoschisis in mice. *Genetics* **186**, 1337-1344 (2010).

55. Anderson MG, *et al*. Genetic context determines susceptibility to intraocular pressure elevation in a mouse pigmentary glaucoma. *BMC Biol* **4**, 20 (2006).

56. Oh J, *et al*. Genetic background-dependent role of Egr1 for eyelid development. *Proc Natl Acad Sci U S A* **114**, E7131-E7139 (2017).

57. Mott R, Flint J. Dissecting quantitative traits in mice. *Annual review of genomics and human genetics* **14**, 421-439 (2013).

813 58. Solberg Woods LC. QTL mapping in outbred populations: successes and challenges.
814 *Physiological genomics* **46**, 81-90 (2014).
815
816 59. Paylakhi S, *et al.* Muller glia-derived PRSS56 is required to sustain ocular axial growth
817 and prevent refractive error. *PLoS Genet* **14**, e1007244 (2018).
818
819

820

821 **Figure 1. *Cctq1* contains two adjacent interacting QTL, *Cctq1a* and *Cctq1b*.** A) The
822 chromosome 7 pairwise scan identified a potential interaction between *D7Mit31* and
823 *rs13479535* (full LOD score = 10.33, interactive LOD score = 5.05). The *upper left triangle*
824 displays the interactive LOD score (LOD_i; left side of the heat map scale) and the *lower right*
825 *triangle* displays the full LOD score (LOD_f; right side of the heat map scale). Chromosome 7
826 positions (Mb) are based on NCBI Build 33. B) Genetic map of chromosome 7 showing the
827 *Cctq1a* and *Cctq1b* loci. The area *boxed in red* is the original *Cctq1* interval blown up to show
828 the intervals of *Cctq1a* and *Cctq1b*, and a subset of the polymorphic markers used for
829 genotyping. The *arrows* indicate the peaks of the two QTL.
830

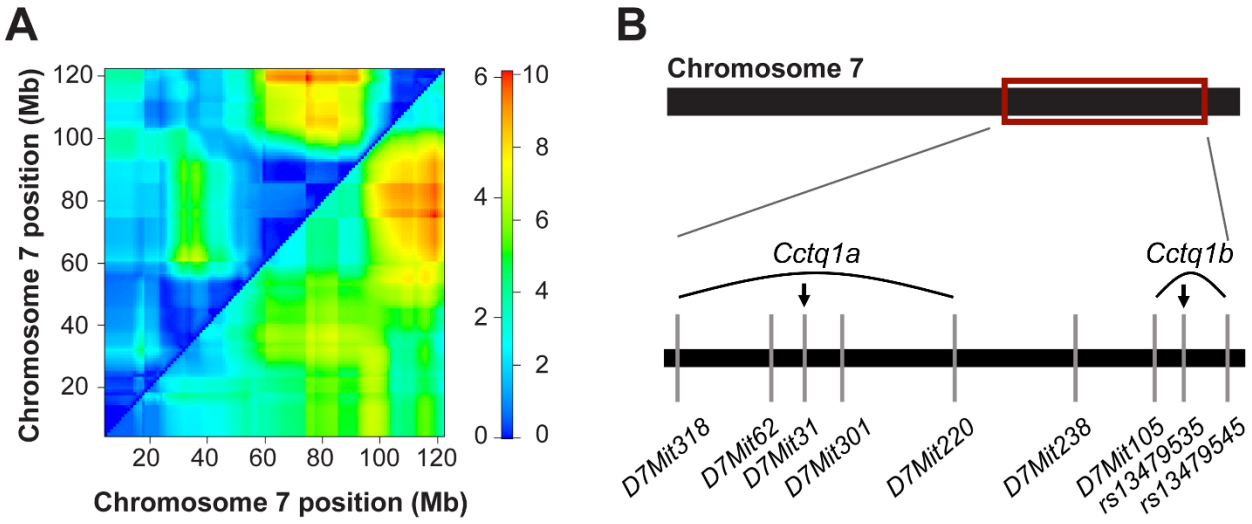

831

832 **Table 1. CCT phenotype results of adult N10F2 mice.**

833

Cctq1a[a]	*Cctq1b*[a]	Avg. CCT ± StDev.[b]	# Mice
KS	KS	94.8 ± 2.4	13
KS	Het	93.3 ± 2.5	13
KS	SJL	90.8 ± 2.6	13
Het	KS	95.5 ± 2.9	13
Het	Het	96.2 ± 3.4	13
Het	SJL	97.0 ± 2.3	13
SJL	KS	88.1 ± 3.7*	13
SJL	Het	86.8 ± 4.2*	13
SJL	SJL	88.8 ± 3.6*	13

834

835 [a] KS, homozygous for KS alleles across the indicated QTL; Het, heterozygous for alleles across

836 the indicated QTL; SJL, homozygous for SJL alleles across the indicated QTL

837 [b] Asterisk (*), significantly different ($p < 0.01$) than inbred KS mice by one-way ANOVA with

838 Tukey post-test

Figure 2. Genetic mapping of *Cctq1a* on mouse chromosome 7 using intercrosses of KS.SJL-*Cctq1a* congenic and sub-congenic mice. *Black boxes* represent the KS or HET genotype associated with a thick cornea and *white boxes* represent the SJL genotype associated with a thin cornea. The number of mice (*n*) with each haplotype is listed to the left of each row, with progeny-tested mice denoted with an asterisk (*). The adult CCT phenotype (*pheno*; measured by optical coherence tomography) relative to littermate controls and the deduced genotype (*geno*) for each haplotype is listed to the right of each row as “Thick KS” or “Thin SJL”. The *vertical lines* across the chromosome represent markers that are polymorphic between KS and SJL mice. Using mice with informative recombinations, the gene underlying *Cctq1a* was narrowed to the region between *rs108403472* and *rs13479393*, which contains seven full genes, *Vmn2r78*, *Vmn2r79*, *Nox4*, *Tyr*, *Grm5*, *Ctsc*, *Rab38*, and *Tmem135*, as well as the 3’ portion of *Vmn2r77* and the 5’ portion of *Fzd4* (*black arrowheads* indicate partial genes).

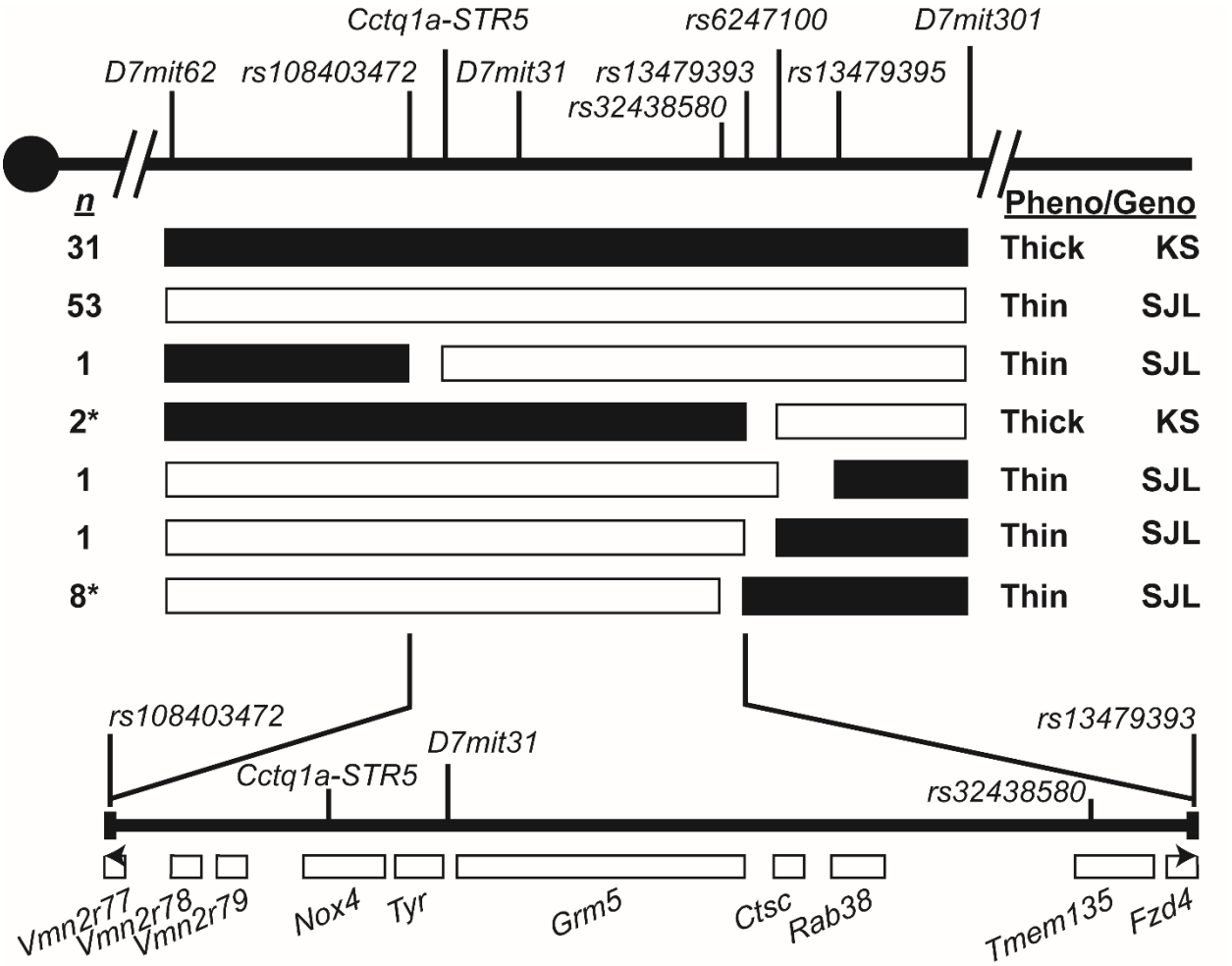

852

Figure 3. Testing the influence of *Cctq1a* lead positional candidate genes on central corneal thickness (CCT). Each point on the graph represents the average CCT measured by optical coherence tomography from one adult mouse with age-matching across genotypes and *error bars* = mean ± standard deviation. A) Homozygosity of *Cctq1a*^{SJL} (*red points*) in KS.SJL-*Cctq1a* N15F7 sub-congenic mice results in a significantly decreased CCT compared to littermate controls having *Cctq1a*^{KS} (*black points*) genotypes ($p < 0.001$; Student's two-tailed *t*-test; 12–13 weeks old). B) The *Fzd4*^{tm1Nat} allele has no effect on CCT, in neither the heterozygous (HET; *blue points*) nor homozygous state (*red points*), compared to *Fzd4* wild-type (WT; *black points*) littermate controls (12–13 weeks old). C) The *Fzd4*^{tm1Nat} allele in trans with a *Cctq1a*^{SJL} allele (*red points*) has no effect on (complements) CCT compared to littermate controls having a *Fzd4*^{WT} allele in trans with a *Cctq1a*^{SJL} allele (*black points*; 17–33 weeks old). D) Homozygosity of the *Ctsc*^{tm1Ley} allele (*red points*) results in a significantly decreased CCT compared to littermate controls (HET = *blue points*; WT = *black points*; $p < 0.002$ for each comparison to homozygotes; one-way ANOVA with Tukey post-test; 11 weeks old). E) The *Ctsc*^{tm1Ley} allele in trans with a *Cctq1a*^{SJL} allele (*red points*) results in a significantly decreased (fails to complement) CCT compared to littermate controls having a *Ctsc*^{tm1Ley} allele in trans with a *Cctq1a*^{KS} allele (*black points*; $p < 0.001$ Student's two-tailed *t*-test; 15–18 weeks old). F) *Ctsc*^{KO} mice on a pure B6 background, harboring one of four *tmMga* alleles (*red points*) predicted to result in a null protein, have an unchanged CCT compared to *Ctsc*^{WT} (*black points*) or *Ctsc*^{HET} (*blue points*) littermate controls (10–12 weeks old). G) The *Ctsc*^{tm1Mga} allele, made on a pure B6 background, in trans with a *Cctq1a*^{SJL} allele (*red points*) has no effect on (complements) CCT compared to littermate controls having a *Ctsc*^{WT} allele in trans with a *Cctq1a*^{SJL} allele (*black points*; 10–11 weeks old). H) Homozygosity of the *Tyr*$^{c-2J}$ allele (*red points*) results in a significantly decreased CCT compared to C57BL/6J mice (*black points*; $p < 0.001$; Student's two-tailed *t*-test; 11–13 weeks old). I) The *Tyr*$^{c-2J}$ allele in trans with a *Cctq1a*^{SJL} allele (*red points*) results in a significantly decreased (fails to complement) CCT compared to

879 littermate controls having a *Tyr*$^{c\text{-}2J}$ allele in trans with a *Cctq1a*^{KS} allele (*black points*; $p < 0.001$;

880 Student's two-tailed *t*-test; 10–12 weeks old).

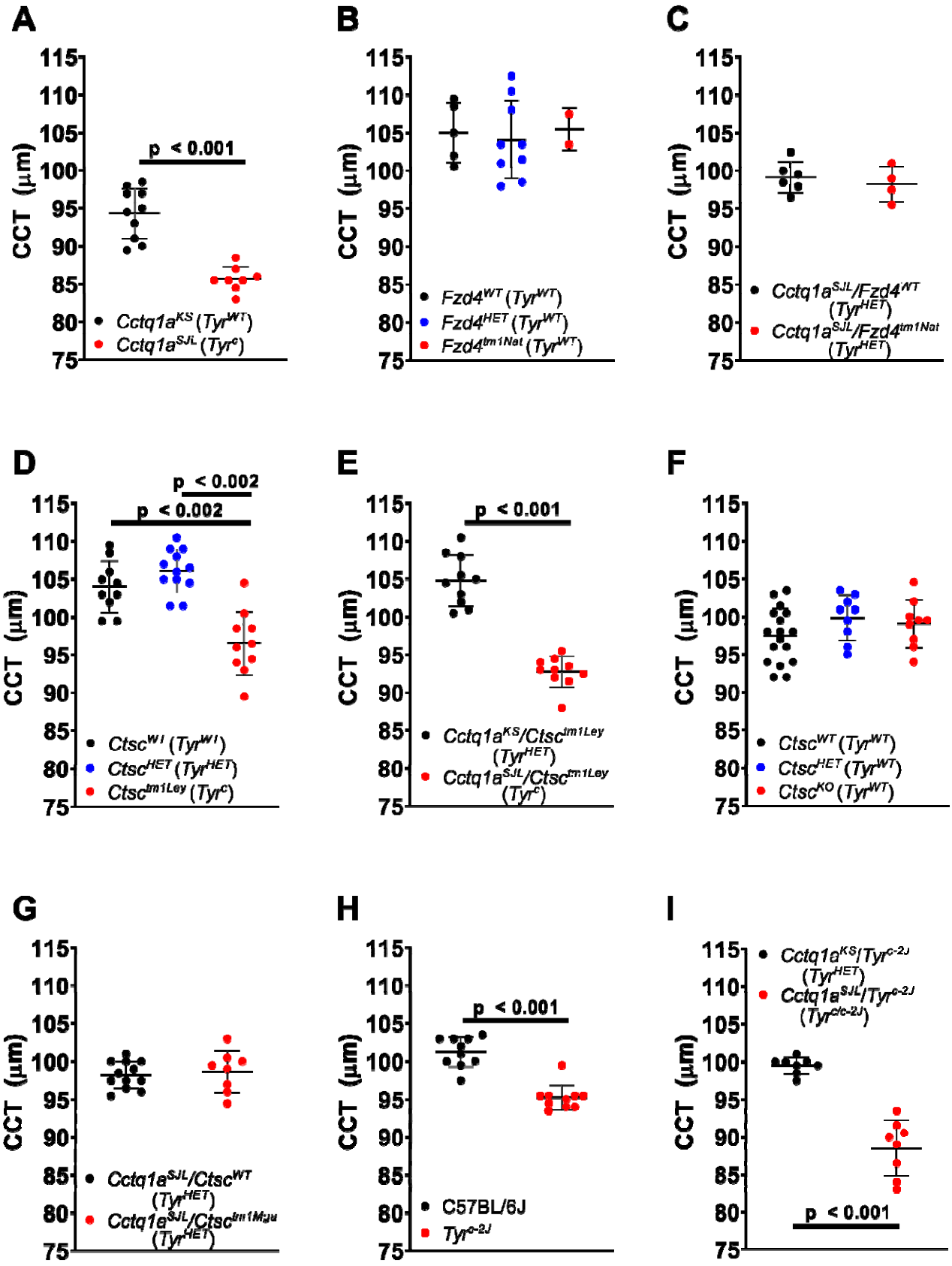

881

882

883 **Figure 4. A null mutation in *Tyr* results in decreased central corneal thickness (CCT).**

884 Each point on the graph represents the average CCT measured by optical coherence

885 tomography from one adult mouse, 13–17 weeks old, with age-matching across genotypes and

886 *error bars* = mean ± standard deviation. Homozygosity of the Tyr^{tm4Mga} allele (*red points*) on a

887 pure C57BL/6J background results in a significantly decreased CCT compared to littermate

888 controls with heterozygous (HET; *blue points*) or wild-type (WT; *black points*) alleles ($p < 0.002$

889 for each comparison to homozygotes; one-way ANOVA with Tukey post-test).

890

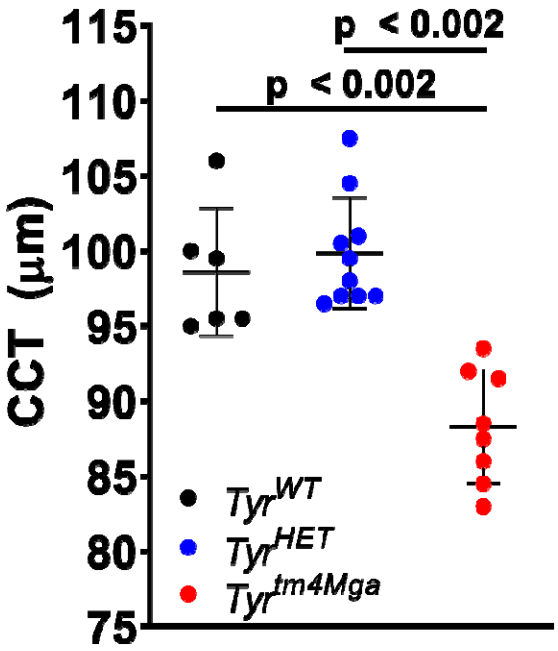

891
892

Figure 5. Testing the influence of DOPA on central corneal thickness (CCT). Each point on the graph represents the average CCT measured by optical coherence tomography from one adult mouse, 13–16 weeks old, with age-matching across genotypes and *error bars* = mean ± standard deviation. Supplemental DOPA supplied in the drinking water from conception through 10-weeks-old has no significant effect on CCT compared to controls in A) C57BL/6J mice, B) *Tyr*$^{c\text{-}h}$ mice, or C) *Tyr*$^{c\text{-}2J}$ mice.

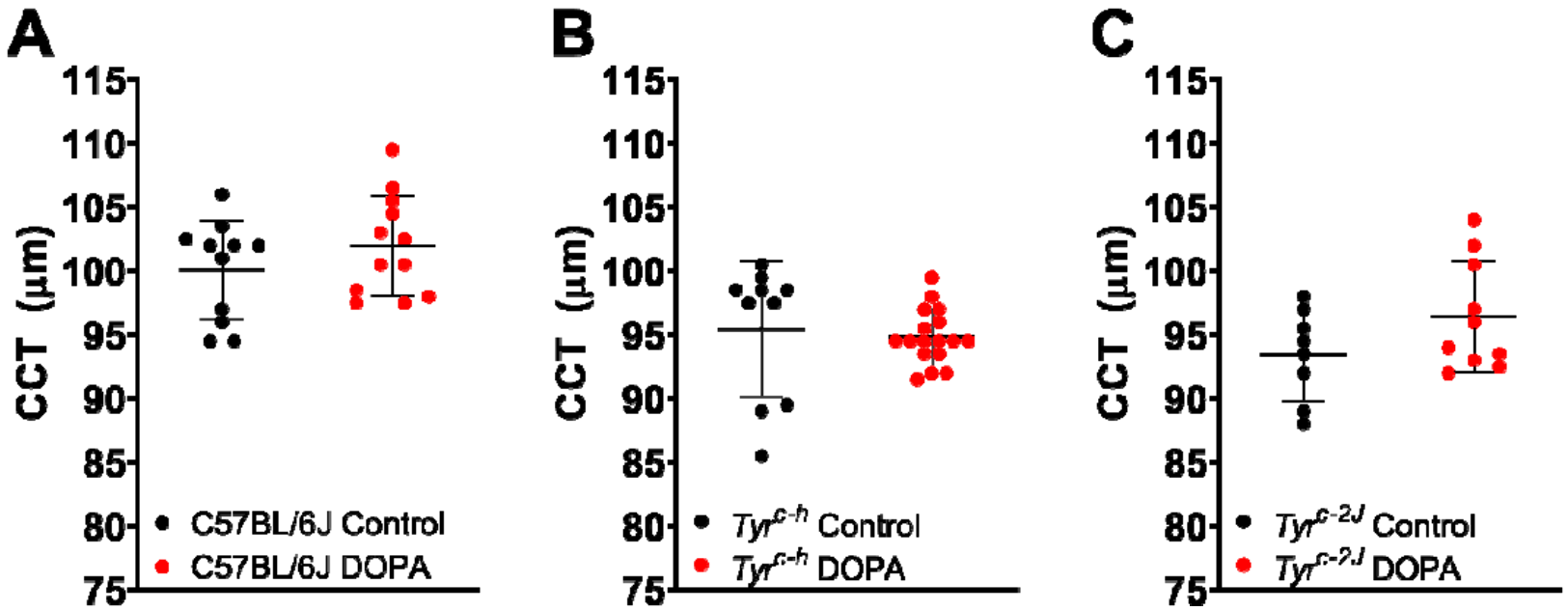

Figure 6. The thin central corneal thickness (CCT) of *c-h* mice raised at increased temperature is rescued by raising *c-h* mice at decreased temperature or by dark-rearing. Each point on the graph represents the average CCT measured by optical coherence tomography from one adult mouse, 10–15 weeks old, with age-matching across genotypes and *error bars* = mean ± standard deviation. Cohorts were subjected to standard lighting (*circles*) or dark-rearing (*diamonds*). Each grouping of *Tyr* genotypes (*black* = WT B6; *blue* = *c-h* temperature sensitive himalayan; *red* = *c-2J* albino) has mice raised at 10°C (*closed points*) or 32°C (*open points*). Note that cold-rearing or dark-rearing *c-h* mice have similar effects that are each statistically significant and that dark-rearing *c-2J* mice significantly changes CCT (one-way ANOVA with Sidak test).

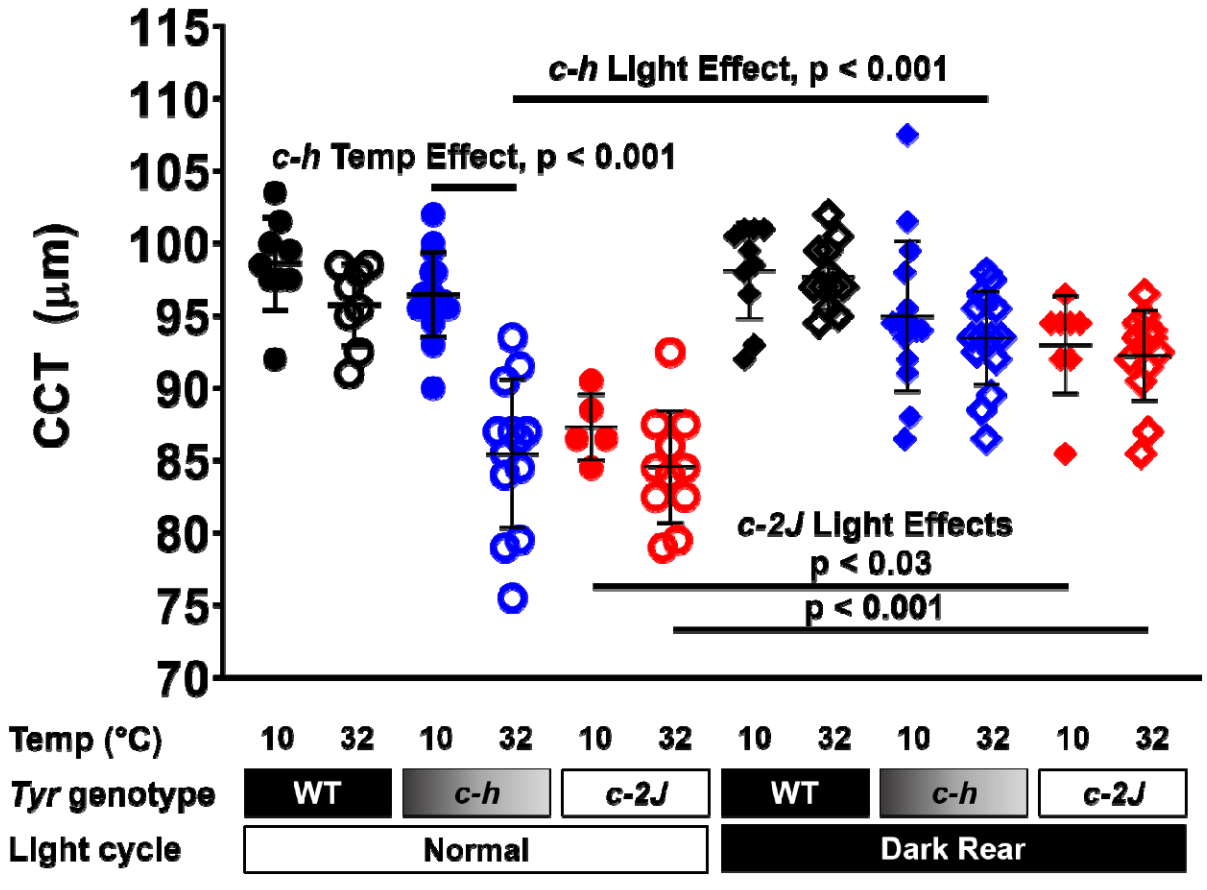

Figure 7. *Tyr* influences ocular axial length. Each point on the graph represents the average axial length measured by optical coherence tomography from one 12-week-old adult mouse and *error bars* = mean ± standard deviation. Axial length differences between C57BL/6J (*black points*) and *Tyr*$^{c\text{-}2J}$ (*red points*) mice, measured from the outer surface of the cornea to the retinal pigment epithelium/choroid interface, are statistically significant ($p < 0.001$; Student's two-tailed *t*-test).